Bioorganic Chemistry 84 (2019) 269–275

Contents lists available at ScienceDirect

Bioorganic Chemistry

journal homepage: www.elsevier.com/locate/bioorg

Phenylpropanoids and lignans from *Prunus tomentosa* seeds as efficient β-amyloid (Aβ) aggregation inhibitors

Qingbo Liu[a,1], Jie Wang[a,1], Bin Lin[b], Zhuo-Yang Cheng[a], Ming Bai[a], Shaochun Shi[a], Xiao-Xiao Huang[a,c], Shao-Jiang Song[a,*]

[a] School of Traditional Chinese Materia Medica, Key Laboratory of Computational Chemistry-Based Natural Antitumor Drug Research & Development, Liaoning Province, Shenyang Pharmaceutical University, Shenyang 110016, People's Republic of China
[b] School of Pharmaceutical Engineering, Shenyang Pharmaceutical University, Shenyang 110016, People's Republic of China
[c] Chinese People's Liberation Army 210 Hospital, Dalian 116021, People's Republic of China

ARTICLE INFO

Keywords:
Phenylpropanoids
Lignans
Prunus tomentosa seeds
Chiral resolution
β-amyloid aggregation

ABSTRACT

Alzheimer's disease (AD) is characterized by the progressive accumulation of extracellular β-amyloid (Aβ) aggregates. Recently, lignans and phenylpropanoids are attracting increasing attention to discovery useful agents of inhibition on Aβ aggregation. In the present study, to develop potential agents for slowing the progression of AD, *Prunus tomentosa* seeds were selected as a raw material for bioactive compounds, which led to the separation of two pairs of new enantiomeric lignans and phenylpropanoids using chiral HPLC. The planar structures of these compounds were elucidated by spectroscopic data analyses. And their absolute configurations were determined by comparing of experimental and calculated electronic circular dichroism (ECD). The biosynthesis pathway was also discussed. Additionally, the inhibitory activity on Aβ aggregation of all optical pure compounds was tested by thioflavin T (ThT) assay. The isolates (**1a**, **1b**, **2a** and **2b**) showed more potent inhibitory activity than positive control curcumin with inhibitory rate of 73.89 ± 3.41% 78.69 ± 1.50%, 63.25 ± 2.68%, and 67.13 ± 0.90% at 20 μM, respectively. More importantly, the inhibition profiles were explained by molecular dynamics and docking simulation studies.

1. Introduction

Alzheimer's disease (AD) is the most common form of neurodegenerative illness, which afflicts more than 40 million suffer worldwide [1,2]. Due to the complex etiology, many factors are suggested to be related to the initiation and development of AD, such as Aβ peptide deposits, hyperphosphorylation of tau protein aggregation, dyshomeostasis of biometals, deficits of acetylcholine (ACh), and oxidative stress [3,4]. Among the various pathogenic factors, the most accepted theory is the cascade hypothesis of Aβ [5], which is believed that the neurotoxicity Aβ deposition-amyloid plagues formed in areas of the brain responsible for pathogenesis of AD. Therefore, the discovery of a lead compound that can inhibit Aβ aggregation has been considered as an effective therapeutic strategy for AD.

Phenylpropanoids and lignans represent large group of naturally occurring phenols, which are widely distributed in the plant kingdom and have a diverse range of medicinal properties including antitumor [6], anti-inflammatory [7], antiviral activity [8]. Additionally, phenylpropanoids and lignans characterized by C6-C3 unit have also been reported to show various effects on AD treatment and are attracting increasing attention [9–11]. During the past several years, a great deal of our efforts has been devoted to discover candidates of anti-AD, which have led to the isolation of lignans with anti-Aβ aggregation activity [12–14].

Prunus tomentosa Thunb. is widely distributed in China, Japan and Korea [15]. Its seeds have been reported to have anti-oxidant and anti-inflammatory activities [16,17]. Previous our phytochemical investigation *P. tomentosa* seeds revealed the presence of lignans with anti-neuroinflammatory effect. In the present study, two new pairs of enantiomers, phenylpropanoids (**1a** and **1b**) and lignans (**2a** and **2b**) were separated from *P. tomentosa* seeds by a chiral chromatographic column. Herein, we described the isolation and structure elucidation of two new pairs of enantiomers. The inhibitory activity on Aβ aggregation was tested by ThT assay. Furthermore, molecular dynamics and docking simulation studies were also carried out to investigate the binding mode of compounds with Aβ.

* Corresponding author.
E-mail address: songsj99@163.com (S.-J. Song).
[1] These authors contributed equally to this work.

https://doi.org/10.1016/j.bioorg.2018.11.041
Received 30 August 2018; Received in revised form 17 November 2018; Accepted 24 November 2018
Available online 26 November 2018
0045-2068/

2. Materials and methods

2.1. General experimental procedures

Optical rotations were measured on a JASCO P-1020 polarimeter (Jasco Co., Tokyo, Japan). The IR data were recorded using a Bruker IFS-55spectrometer. The UV spectra were obtained with a Shimadzu UV-1700 spectrometer. The ECD spectra were performed on an MOS 450 detector from BioLogic (Claix, France). HRESIMS experiments were conducted using a MicroTOF spectrometer (Bruker Co., Karlsruhe, Germany). The ^{1}H and ^{13}C NMR spectra were recorded on Bruker DPX-400 (Bruker Co., Billerica, MA, USA). Semi-preparative HPLC was performed on a Waters 1525 instrument (UV 2549 detector) using an YMC C18 column (250 mm × 10 mm, 5 μm). The Chiralpak C column (4.6 × 250 mm, 5 μm, Daicel Polymer Ltd., Tokyo, Japan) and Chiralpak IG column (4.6 × 250 mm, 5 μm, Daicel Polymer Ltd., Tokyo, Japan) were used in the HPLC system. Column chromatography was performed on macroporous resin (D101, Baoen Chemical Co., Cangzhou, China), silica-gel (100–200 or 200–300 mesh, Qingdao Marine Chemistry Ltd., Qingdao, China) and octadecylsilane (ODS) (40–80 μm, Nacalai Tosoh, Inc., Uetikon, Switzerland). $A\beta_{1\text{-}42}$ was purchased from Aladdin (Qigang Rd, Fengxian, Shanghai).

2.2. Plant material

The *P. tomentosa* seeds were supplied by a wine manufacturing company from Liaoning Province, PR China, on July 18, 2012. A voucher specimen (No. 20120718) was deposited in the Herbarium of Shenyang Pharmaceutical University, Liaoning, PR China.

2.3. Extraction and isolation

The dried and powdered seeds of *P. tomentosa* (15 kg) were extracted three times with 70% EtOH. After evaporation of the solvent under vacuum, a brown-dark residue of 650 g was obtained. This residue was suspended in H_2O and partitioned successively with petroleum ether, EtOAc and *n*-BuOH. The EtOAc fraction (70 g) was subjected to polyamide column chromatography (CC) eluting successively with MeOH-H_2O (30:70, 50:50, 70:30, 100:0, v/v) to yield 4 fractions (Fr.E1–Fr.E4). Fr.E1 (26 g) was separated by ODS-gel CC eluting with a gradient of MeOH-H_2O (20:80, 40:60, 100:0, v/v) to give 3 sub-fractions (Fr.E1-1–E1-3). Fr. E1-1 (12 g) was loaded onto silica-gel CC using MeOH-H_2O (50:1–5:1, v/v), and then purified by RP-HPLC (MeOH-H_2O) to obtain **1** (5.5 mg) and **2** (6.3 mg). Subsequently, Chiral resolution of **1** was performed on a Daicel Chiralpak IC column (eluted with *n*-hexane: 2-propanol, 83:17, v/v, flow rate 0.4 mL/min, detection wavelength UV 254 nm) to obtain **1a** (2.0 mg, t_R = 53 min) and **1b** (2.5 mg, t_R = 74 min). **2** (6.3 mg) was separated by Daicel Chiralpak IG column (eluted with MeCN–H_2O, v/v, 20:80, flow rate 0.5 mL/min, detection wavelength UV 254 nm) to give **2a** (2.6 mg, t_R = 22 min) and **2b** (2.1 mg, t_R = 30 min) (Fig. 1).

1-(3,5-dimethoxy-4-hydroxyphenyl)-2-(3-methoxy-4-hydroxyphenyl)-3-hydroxy-propan-1-one ***(1)****:* yellow oil; UV (MeOH) λ_{max} (logε): 231 (0.64), 278 (0.34), 307 (0.30); HRESIMS at *m/z* 371.1102 $[M+Na]^+$ (calcd 371.1101); ^{1}H and ^{13}C NMR, see Table 1.

Table 1
^{1}H NMR (400 MHz) and ^{13}C NMR (100 MHz) data in CD_3OD for **1** and **2**.

Position	1		2	
	δ_H	δ_C	δ_H	δ_C
1		198.1		196.1
2	4.77 (dd, *J* = 8.8, 5.2 Hz)	55.0	5.54 (t, *J* = 4.8 Hz)	82.6
3	4.27 (dd, *J* = 11.2, 8.8 Hz) 3.73 (dd, *J* = 11.2, 5.2 Hz)	64.0	4.04 (2H, m)	63.0
1′		127.4		127.3
2′	7.38 (brs)	106.5	7.64 (d, *J* = 2.0 Hz)	111.3
3′		148.0		147.6
4′		141.0		152.5
5′		148.0	6.89 (d, *J* = 8.4 Hz)	114.6
6′	7.38 (brs)	106.5	7.71 (dd, *J* = 8.4, 2.0 Hz)	123.7
1″		128.6		136.8
2″	6.93 (d, *J* = 1.6 Hz)	111.3	6.85 (d, *J* = 1.6 Hz)	112.7
3″		147.5		149.7
4″		145.6		145.1
5″	6.75 (d, *J* = 8.0 Hz)	115.3	6.78 (d, *J* = 8.0 Hz)	116.4
6″	6.79 (dd, *J* = 8.0, 1.6 Hz)	120.8	6.67 (dd, *J* = 8.0, 1.6 Hz)	120.2
7″			2.62 (2H, t, *J* = 7.6 Hz)	34.1
8″			1.80 (2H, m)	31.2
9″			3.55 (2H, t, *J* = 6.4 Hz)	60.7
3′-OCH_3	3.86 (s)	55.4	3.90 (s)	55.0
5′-OCH_3	3.86 (s)	55.4		
3″-OCH_3	3.83 (s)	55.1	3.80 (s)	54.9

The coupling constants (*J*) were in parentheses and reported in Hz; chemical shifts were given in ppm.

(S)-1 ***(1a)****:* [α]20 D-52 (*c* 0.10, MeOH); ECD (*c* 1.0 mg/mL, MeOH) λ_{max} ($\Delta\varepsilon$) 237 (−31.15), 274 (+22.78), 309 (−27.21) nm.

(R)-1 ***(1b)****:* [α]20 D +50 (*c* 0.10, MeOH); ECD (*c* 1.0 mg/mL, MeOH) λ_{max} ($\Delta\varepsilon$) 237 (+27.12), 274 (–22.03), 309 (+22.82) nm.

1-(3-methoxy-4-hydroxyphenyl)-2-(3-methoxy-1-hydroxypropylphenoxy)-3-hydroxy-propan-1-one ***(2)****:* colorless oil; UV (MeOH) λ_{max} (logε): 230 (0.68), 282 (0.39), 308 (0.32); HRESIMS at *m/z* 399.1420 $[M+Na]^+$ (calcd for $C_{20}H_{24}O_7Na$, 399.1414); ^{1}H and ^{13}C NMR, see Table 1.

(R)-2 ***(2a)****:* [α]20 D-17 (*c* 0.10, MeOH); ECD (*c* 1.0 mg/mL, MeOH) λ_{max} ($\Delta\varepsilon$) 233 (+4.81), 275 (−15.67), 333 (+4.38) nm.

(S)-2 ***(2b)****:* [α]20 D +16 (*c* 0.10, MeOH); ECD (*c* 1.0 mg/mL, MeOH) λ_{max} ($\Delta\varepsilon$) 231 (-9.91), 272 (+10.25), 330 (-5.49) nm.

2.4. ECD calculations

The absolute configuration of compounds **1** and **2** were determined by using time-dependent density functional theory (TDDFT) calculations [18]. Conformational searches were performed by employing MMFF94S force field using CONFLEX [19]. Those predominant geometries with their energies less than 3 kcal/mol relative to the conformation with the lowest energy were selected for the further geometry optimization at the B3LYP/6-31G(d) level. The ECD of the conformers were calculated by the TDDFT method at the B3LYP/6-311++G(2d,p) levels with the CPCM model in methanol solution, and the overall calculated ECD curves were generated using SpecDis 1.51 [20].

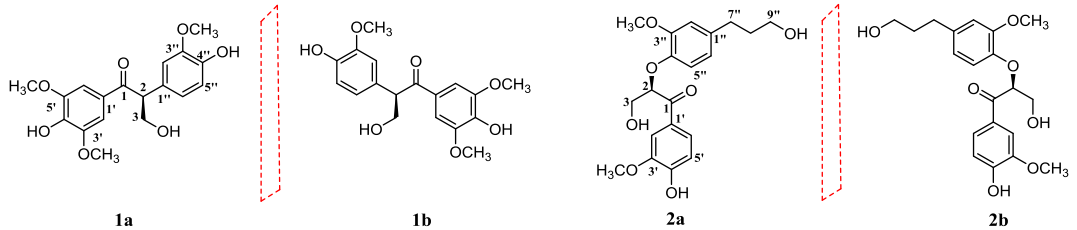

Fig. 1. Chemical structures of compounds **1a**/**1b**−**2a**/**2b**.

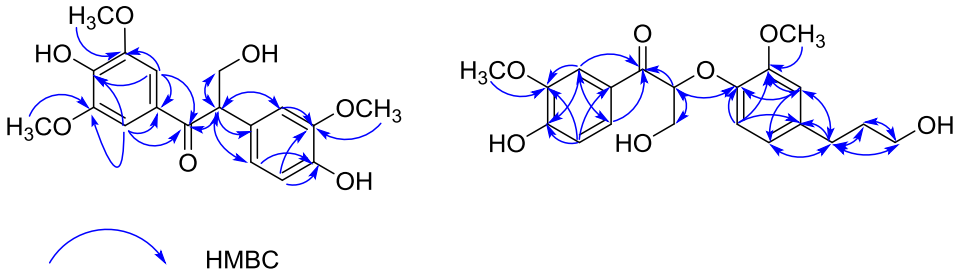

Fig. 2. Key HMBC correlations of compounds **1** and **2**.

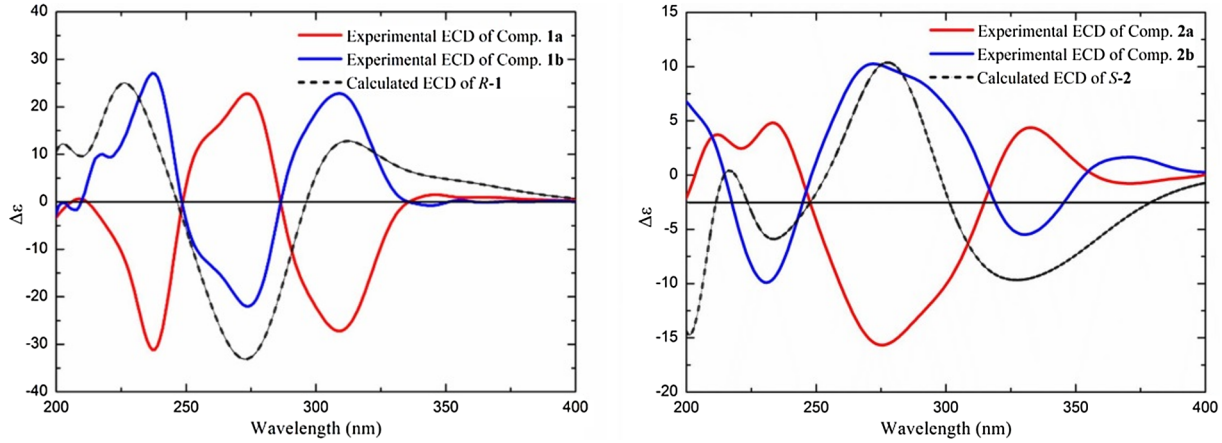

Fig. 3. Calculated and experimental ECD spectra of **1a**/**1b** and **2a**/**2b**.

2.5. Inhibition of self-induced $A\beta_{1\text{-}42}$ aggregation

These compounds were performed to evaluate for their ability of inhibiting $A\beta_{1\text{-}42}$ aggregation by ThT assay, using curcumin as a positive control. The stable stock solutions of prepared $A\beta_{1\text{–}42}$ (25 μM in PBS, 10 μL) and the tested compounds (160 μM in PBS, 10 μL) were added to 80 μL phosphate-buffered saline (PBS) at pH 7.4. Then 1 μL of each compound and 9 μL of 25 μM $A\beta_{1\text{–}42}$ sample were added to the 96-well plates and the final concentration of each compound was 20 μM, and samples were prepared in triplicate. The plates were covered to minimize evaporation and incubated in the dark at 37 °C for 24 h. After incubation, 80 μL of 5 μM ThT was added to each well. Fluorescence was measured using a Varioskan Flash Multimode Reader instrument (Thermo Scientific, USA) with excitation and emission wavelengths of 450 nm and 485 nm, respectively.

2.6. ECD studies

A solution of 50 μM $A\beta_{1\text{–}42}$ peptide, in the absence or presence of 50 μM **1b** was incubated at 37 °C. ECD measurements were recorded in a wavelength range of 190 and 250 nm according to the reported methods [21,22].

2.7. Molecular dynamic simulations

MD simulations were performed with GROMACS5 package using CHARMM36 force field [23]. The X-ray crystal structure code of the protein $A\beta_{1\text{–}42}$ (PDB: 1IYT) was obtained from Protein Data Bank. The protein structure was solvated in a cubic box of size 7.25 nm with 12,651 TIP3P water molecules. The protein structure was placed in a cubic box of dimension 7.25 nm with 12,651 TIP3P water molecules. The minimum distance from the complex to the edge of the box was kept 1 nm [24]. Sodium and chloride ions were added to neutralize the system, which was equilibrated over 10 ns while progressively releasing position restraints on the protein atoms. Temperature and pressure were allocated at 298 K and 1.01325 bar, respectively using Isothermal-isobaric (NPT) ensemble. Cut-off radios of 9 Å was applied for Coulomb interactions [25].

2.8. Molecular docking

These structures were performed for the molecular modeling calculations and docking studies using Molegro Virtual Docker 4.40 program (Molegro). The X-ray crystal structure code of the protein $A\beta_{1\text{-}42}$ from Protein Data Bank was 1IYT. The protein structure was optimized by the Discovery Studio 4.3 program to add all hydrogen atoms and remove water molecules.

2.9. Statistical analysis

All the presented data and results were confirmed in at least three independent experiments. Error bars express the standard deviation (S.D.). Statistical analysis of data was made by the student *t*-test (Graphpad Prism 6 software). All the data show a normal distribution. $P < 0.05$ is considered statistically significant.

3. Results and discussion

3.1. Phytochemical investigation

Compound **1** was isolated as yellow oil. The molecular formula was established as $C_{18}H_{20}O_7$ on the basis of its HRESIMS ion peak at *m/z* 371.1102 $[M+Na]^+$ (calcd for $C_{18}H_{20}O_7Na$, 371.1101), indicating the presence of 9 degrees of unsaturation. Its UV spectrum exhibited maximum absorption bands at λ_{max} 231, 278, 307 nm. The ^1H NMR data (Table 1) showed two aromatic protons at δ_H 7.38 (2H, s, H-2′,6′), and an ABX spin system at δ_H 6.93 (1H, d, J = 1.6 Hz, H-2″), 6.79 (1H, dd, J = 8.0, 1.6 Hz, H-6″), 6.75 (1H, d, J = 8.0 Hz, H-5″), indicating the existence of a symmetrical 1,3,4,5-tetrasubstituted benzene system and a 1,3,4-trisubstituted benzene system. A hydroxymethyl group was

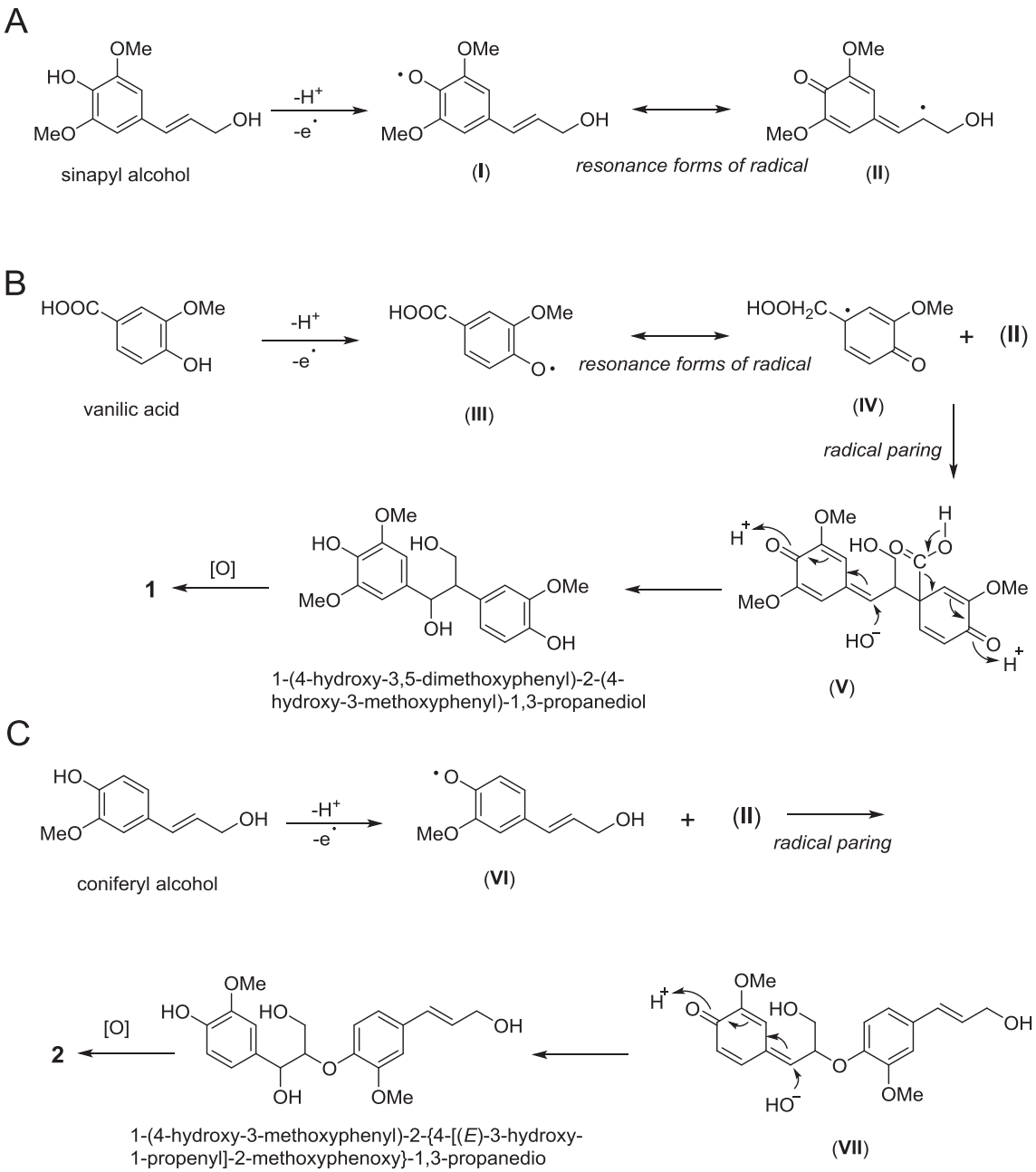

Scheme 1. Proposed biosynthesis of compounds **1** and **2**.

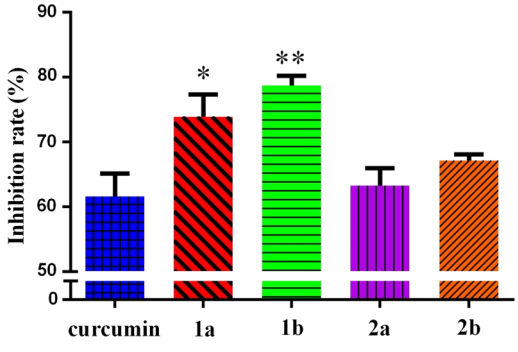

Fig. 4. Inhibitory rate of the isolates for self-induced $A\beta_{1-42}$ aggregation at 20 μM. The inhibitory rate (%) was showed as mean ± SD of three independent experiments. *P < 0.05, **P < 0.01, versus the positive control.

determined by the remaining signals at δ_H 4.27 (1H, dd, J = 11.2, 8.8 Hz, H-3a), 3.73 (1H, dd, J = 11.2, 5.2 Hz, H-3b), Additionally, a methine group at δ_H 4.77 (1H, dd, J = 8.8, 5.2 Hz, H-2) and three methoxyl groups at δ_H 3.86 (6H, s, H-3′,5′), 3.83 (3H, s, H-3″) were also observed. The ^{13}C NMR data displayed 18 carbon signals including a carbonyl carbon, 12 aromatic carbons, an oxygenated methylene carbon, and 3 methoxy groups. Detailed comparison of the NMR data of **1** (Table 1) with the known compound [26] revealed that compound **1** is a 1,2-diarylpropane type phenylpropanoid with more two methoxy groups at C-3′/5′. The HMBC correlations (Fig. 2) of H-2′,6′/C-1 and H-2/C-1 indicated that a ketone carbonyl (δ_C 198.1) is linked to C-1. The correlations of H-2/C-1″, C-2″ and C-6″ suggested the direct linkage of C-2 to C-1″. Additionally, the HMBC spectrum showed the correlations from δ_H 3.86 to C-3′/5′ (δ_C 148.0) and from δ_H 3.83 to C-3″ (δ_C 147.5), which revealed the position of the three methoxy groups. From all the above evidence, the chemical structure of **1** was established as 1-(3,5-dimethoxy-4-hydroxyphenyl)-2-(3-methoxy-4-hydroxyphenyl)-3-

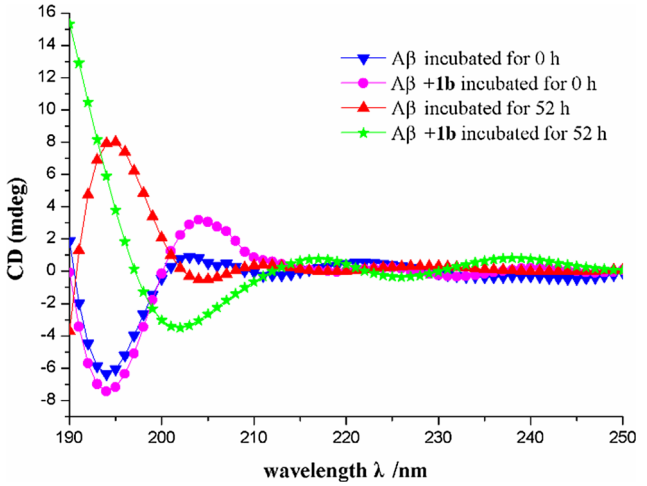

Fig. 5. ECD spectra of Aβ_{1-42} (50 μM) and a 1:1 mixture of 50 μM **1b** and 50 μM Aβ_{1-42} incubated for 52 h at 37 °C. Spectra for Aβ_{1-42} alone and the 1:1 mixture were obtained at t = 0 h (blue and pink, respectively), and after 52 h incubation (red and green, respectively).

hydroxy-propan-1-one.

The weak Cotton effects in its ECD spectrum and measurable optical rotation suggested that compound **1** was a racemic mixture. To confirm this, a chiral HPLC analysis was carried out, revealing the presence of two chromatographic peaks to prepare optically pure **1a** and **1b**, which showed anticipated mirror-imaged ECD curves (Fig. 3). Their absolute configurations were confirmed by comparison of its experimental and calculated ECD spectra at the B3LYP/6-311 + + G(2d,p) level with the CPCM model in methanol solution. Compound **1b** showed positive cotton effects at 237 nm ($\Delta\varepsilon$ + 27.11), 309 nm ($\Delta\varepsilon$ + 22.81) and negative cotton effect at 274 nm ($\Delta\varepsilon$ −22.03) which matched well with the calculated ECD spectrum for *R*-**1** showed in Fig. 3. The UV spectrum of **1** showed a strong absorption at λ_{max} 231 nm attributable to the benzoyl moiety. Thus, the absolute confguration of **1a** and **1b** was unambiguously assigned as (*S*)-1-(3,5-dimethoxy-4-hydroxyphenyl)-2-(3-methoxy-4-hydroxyphenyl)-3-hydroxy-propan-1-one and (*R*)-1-(3,5-dimethoxy-4-hydroxyphenyl)-2-(3-methoxy-4-hydroxyphenyl)-3-hydroxy-propan-1-one, respectively.

Compound **2** was obtained as a colorless oil, and its molecular formula was determined as $C_{20}H_{24}O_7$ from the HRESIMS ion peak at *m/z* 399.1420 $[M + Na]^+$ (calcd for $C_{20}H_{24}O_7Na$, 399.1414), corresponding to 9 degrees of unsaturation. The UV spectrum showed the absorption maxima at λ_{max} 230, 282 and 308 nm. The ^{1}H NMR data of **2** displayed the presence of two 1,3,4-trisubstituted benzene system [δ_H 7.64 (1H, d, J = 2.0 Hz, H-2′), 7.71 (1H, dd, J = 8.4, 2.0 Hz, H-6′), 6.89 (1H, d, J = 8.4 Hz, H-5′); 6.85 (1H, d, J = 1.6 Hz, H-2″), 6.67 (1H, dd, J = 8.0, 1.6 Hz, H-6″), 6.78 (1H, d, J = 8.0 Hz, H-5″)]. The ^{13}C NMR data of **2** displayed 20 carbon signals including a ketone carbonyl at δ_C 196.1 (C-1). A comparison of NMR data of **2** with that of **1** revealed that a methine group (δ_C 55.0) in **1** was replaced by an oxygenated methine group (δ_C 82.6), and the additional hydroxypropyl group of **2** was linked to the aromatic ring. The aforementioned information showed high similarity with the known compound [27] indicating that compound **2** has an 8-*O*-4′ neolignan skeleton. The HMBC correlations (Fig. 2) of H-7″ with C-2″ and C-6″ confirmed that a hydroxypropyl group is linked to C-1″. The chemical structure of **2** was then identified as 1-(3-methoxy-4-hydroxyphenyl)-2-(3-methoxy-1-hydroxypropyl-phenoxy)-3-hydroxy-propan-1-one.

Compound **2** was also found to be a racemic mixture, and was further resolved to yield **2a** and **2b** over HPLC using a chiral column exhibited mirror image-like ECD curves (Fig. 3). The ECD spectrum of **2b** showed negative cotton effects at 231 nm ($\Delta\varepsilon$ −9.91), 330 nm ($\Delta\varepsilon$ −5.49) and positive cotton effect at 272 nm ($\Delta\varepsilon$ + 10.25), matching very well with the calculated ECD curve of *S*-**2** at the B3LYP/6–311 + + G(2d,p) level with the CPCM model. Thus, the absolute configurations of **2a** and **2b** were assigned as (*R*)-1-(3-methoxy-4-hydroxyphenyl)-2-(3-methoxy-1-hydroxypropylphenoxy)-3-hydroxy-propan-1-one and (*S*)-1-(3-methoxy-4-hydroxyphenyl)-2-(3-methoxy-1-hydroxypropylphenoxy)-3-hydroxy-propan-1-one, respectively.

A possible biogenesis pathway of isolates **1** and **2** was shown in Scheme 1. These two compounds belong to different type secondary metabolites, but they are proposed to undergo similar biogenesis pathway including radical pairing and subsequent oxidation. Interestingly, the two compounds share a common allyl C-radical intermediate (**II**) formed by sinapyl alcohol, which has been reported as a precursor of many lignans and phenylpropanoids [28,29].

3.2. Inhibition of self-induced Aβ_{1-42} aggregation

To investigate the effect of these promising compounds to inhibit the self-induced Aβ_{1-42} aggregation, the Thioflavin T (ThT) fluorescence assay was performed, with curcumin as a positive control [30,31]. From the results summarized in Fig. 4, compounds **1a** and **1b** exhibited significant inhibitory effect (73.89 ± 3.41% and 78.69 ± 1.50%, respectively) of Aβ_{1-42} aggregation at a concentration of 20 μM. Compounds **2a** and **2b** showed moderate anti-Aβ_{1-42} aggregation activities with inhibition rates of 63.25 ± 2.68%, and 67.13 ± 0.90%, respectively. Among them, the inhibitory activity of the compound **1b** was higher than the reference compound curcumin (61.56 ± 3.55%). To explain these observations, molecular dynamics and docking studies were carried out.

ECD can be a very important tool to characterise protein-ligand interaction and protein aggregation [32]. To support the findings of the thioflavin-T binding assay, the inhibition of Aβ_{1-42} aggregation was also confirmed by ECD. Promising compound **1b** was further chosen to performed this assay for its optimal Aβ_{1-42} aggregation inhibition capability. As shown in Fig. 5, ECD spectrum of monomeric Aβ_{1-42} and an equal proportion of **1b**/Aβ_{1-42} showed a negative band around 195 nm at 0 h. After 52 h of incubation, ECD spectra of aggregated Aβ_{1-42} shifted to have a positive band around 195 nm, indicating the transition of the Aβ_{1-42} from a statistical coil to β-sheet rich conformation. On the other hand, the ECD spectrum of the 1:1 solution only displayed minima slightly red shifted at *ca.* 202 nm compared to non-aggregated Aβ_{1-42}. Overall, CD results substantiate that the addition of **1b** may reduce the structural transition in Aβ_{1-42} towards the formation of β-sheet structure.

In order to obtain further insight into the mechanism of Aβ_{1-42} aggregated inhibition, molecular docking simulation were carried out to explore the possible the binding modes of compounds **1a**/**1b** and **2a**/**2b** and key interactions with Aβ_{1-42} monomer residues [33]. Previous investigation of protein-ligand interaction using docking, the molecular dynamics simulation was performed for the protein system using GROMACS5 package to relax the structure and dynamics of protein. The result was used for further docking simulations. Comparison with the molecular docking models in Fig. 6 showed that the 7-carbonyl, 5-methoxyl, 4-hydroxy and 4′-hydroxy of compound **1b** were bound to the Tyr10, Gln15, Glu11 and Gly9 residues of Aβ_{1-42} via five hydrogen bonding interactions (distance 2.51 Å, 1.66 Å, 2.35 Å, 1.92 Å and 1.94 Å, respectively) and the benzene ring of **1b** was bound to the Tyr 10 residue (distance 4.77 Å) of Aβ_{1-42} via π–π stacking interaction. Meanwhile, there were four hydrogen bonds between the 7-carbonyl and 4′-hydroxy of compound **1a** and the Leu17, Val18, Gln15 and Glu11 residues of Aβ_{1-42} (distance 2.59 Å, 2.45 Å, 1.54 Å, 2.58 Å, respectively), and there were also π–π stacking interactions between the benzene ring of compound **1a** and Tyr 10 residue of Aβ_{1-42}. Moreover, in comparison with **1a**/**1b**, **2a**/**2b** exhibited two or three hydrogen bonding interactions with Aβ_{1-42}. These results combined their inhibitory activity indicated that hydrogen bonding interactions played an important role than the other weak intermolecular force in the

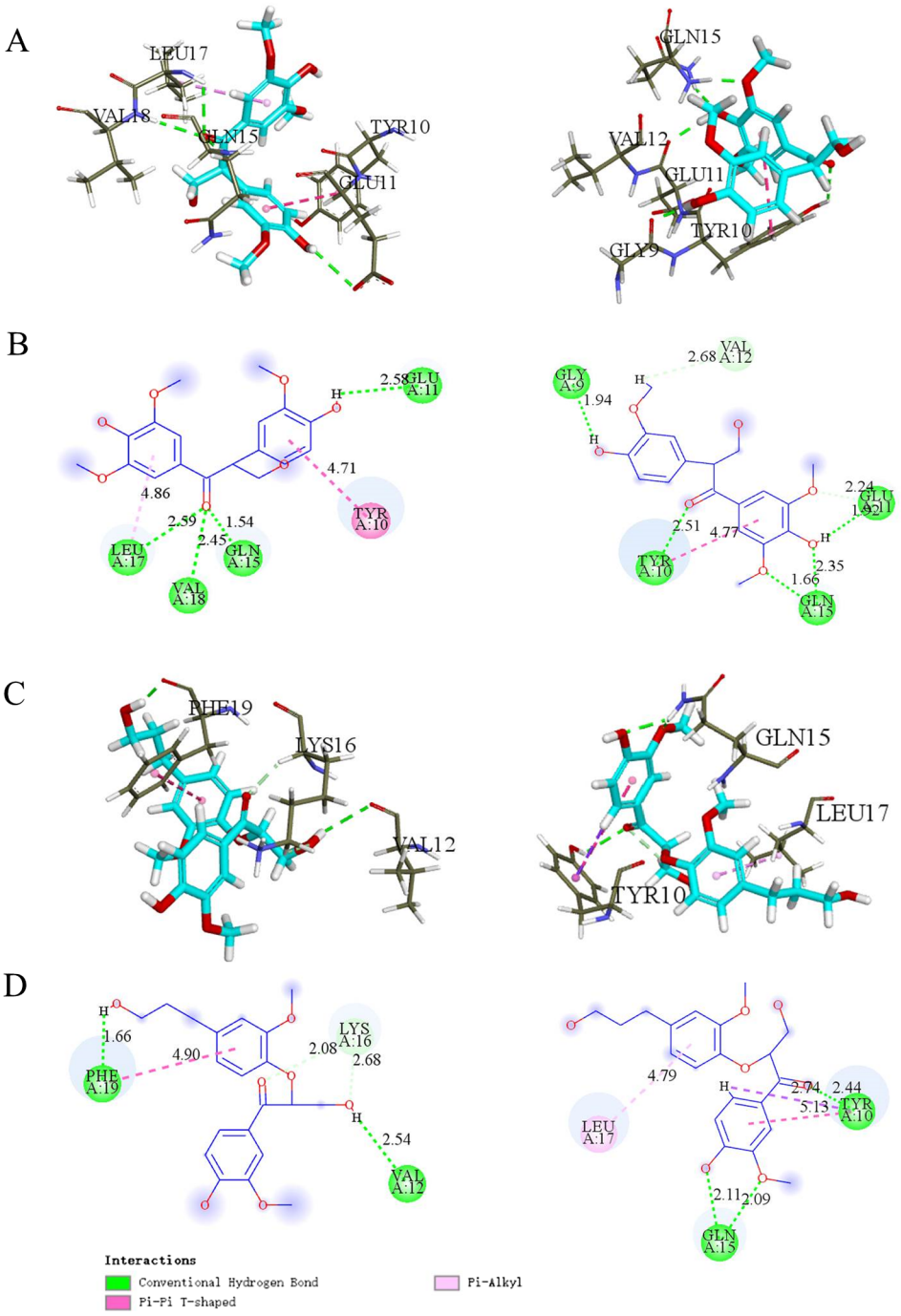

Fig. 6. Docking models of compounds **1a/1b** and **2a/2b** with Aβ_{1-42} (PDB code: 1IYT). A: H-bonding and other interactions of compounds **1a/1b** and Aβ_{1-42}. B: 2D schematic diagram of compounds **1a/1b** and Aβ_{1-42}. C. H-bonding and other interactions of compounds **2a/2b** and Aβ_{1-42}. D: 2D schematic diagram of compounds **2a/2b** and Aβ_{1-42}.

stability of the complex [34]. Since positive control curcumin shared many structural similarities to the compounds **1a/1b**, **2a/2b**. Further comparison of isolated compounds and curcumin (binding mode see supplementary information) interactions with Aβ_{1-42} in docking simulation was carried out. As a result, these investigated compounds shared a common hydrogen bond with residue Gln15 in Aβ_{1-42}, and also this residue has been reported as a key active site interacting with other natural ligands [35]. Overall, the results in docking study were consistent with ThT assay, and further proved that compound **1b** showed a degree of optical selectivity on Aβ_{1-42} aggregated inhibition.

In summary, to develop potential agents for slowing the progression of AD, two new pairs of enantiomeric phenylpropanoids (**1a/1b)** and lignans (**2a/2b**) from *P. tomentosa* seeds were identified. And their absolute configurations were determined by comparison of its experimental and calculated ECD spectrum. Notably, the inhibition of self-induced Aβ_{1-42} aggregation activity was evaluated, and all optical pure compounds exhibited more potent inhibitory activity than positive control curcumin. Docking simulation study exhibits that the Gln15 may be a key active residue for isolates against self-induced Aβ_{1-42} aggregation. These findings indicated that the *P. tomentosa* seeds could

be developed as a medicinal supplement to prevent and treat diseases related to neuron degeneration and damage. In the future, we intend to investigate new physiological functions of lignans and phenylpropanoids isolated from *P. tomentosa* seeds in more detail through both *in vitro* and *in vivo* studies.

Conflicts of interest

The authors declare no competing financial interest.

Acknowledgements

This work was supported by the Project of Innovation Team (LT2015027) of Liaoning of P.R. China.

Appendix A. Supplementary material

Supplementary data to this article can be found online at https://doi.org/10.1016/j.bioorg.2018.11.041.

References

[1] T. Huang, H.T. Zhao, S.M. Zhong, Z.Y. Wang, Z.F. Chen, L. Hong, Novel oxoisoaporphine-based inhibitors of acetyl- and butyrylcholinesterase and acetylcholinesterase-induced β-amyloid aggregation, Bioorg. Med. Chem. Lett. 22 (2012) 2257–2261.
[2] G. Tommonaro, N. Garcíafont, R.M. Vitale, B. Pejin, C. Iodice, S. Cañadas, J. Marcocontelles, M.J. Osetgasque, Avarol derivatives as competitive AChE inhibitors, non hepatotoxic and neuroprotective agents for Alzheimer's disease, Eur. J. Med. Chem. 122 (2016) 326–338.
[3] E. Scarpini, P. Scheltens, H. Feldman, Treatment of Alzheimer's disease: current status and new perspectives, Lancet. Neurol. 2 (2003) 539–547.
[4] A. Cavalli, M.L. Bolognesi, A. Minarini, M. Rosini, V. Tumiatti, M. Recanatini, C. Melchiorre, Multi-target-directed ligands to combat neurodegenerative diseases, J. Med. Chem. 51 (2008) 347–372.
[5] A. Boutajangout, T. Wisniewski, Tau-based therapeutic approaches for Alzheimer's disease - a mini-review, Gerontology 60 (2014) 381–385.
[6] K.L. Allen, D.R. Tschantz, K.S. Awad, W.P. Lynch, A.L. Delucia, A plant lignan, 3′-*O*-Methyl-Nordihydroguaiaretic acid, suppresses papillomavirus E6 protein function, stabilizes p53 protein, and induces apoptosis in cervical tumor cells, Mol. Carcinogen. 46 (2010) 564–575.
[7] C.S. Kim, O.W. Kwon, Y.K. Sun, R.L. Kang, Bioactive Lignans from the Trunk of *Abies holophylla*, J. Nat. Prod. 76 (2013) 2131–2135.
[8] G.Y. Yang, Y.K. Li, R.R. Wang, X.N. Li, W.L. Xiao, L.M. Yang, J.X. Pu, Y.T. Zheng, H.D. Sun, Dibenzocyclooctadiene lignans from *Schisandra wilsoniana* and their anti-HIV-1 activities, J. Asian. Nat. Prod. Res. 13 (2011) 592–598.
[9] X.H. Luo, Y.Y. Zhang, X.Y. Chen, M.L. Sun, S. Li, H.B. Wang, Lignans from the roots of *Acorus tatarinowii* Schott ameliorate β amyloid-induced toxicity in transgenic *Caenorhabditis elegans*, Fitoterapia 108 (2016) 5–8.
[10] Z.Q. Zhou, J. Xiao, H.X. Fan, Y. Yu, R.R. He, X.L. Feng, H. Kurihara, K.F. So, X.S. Yao, H. Gao, Polyphenols from wolfberry and their bioactivities, Food. Chem. 214 (2017) 644–654.
[11] S. Katayama, H. Sugiyama, S. Kushimoto, Y. Uchiyama, M. Hirano, S. Nakamura, Effects of sesaminol feeding on brain Aβ accumulation in a senescence-accelerated mouse-prone 8, SAMP8, J. Agr. Food. Chem. 64 (2016) 4908–4913.
[12] X.X. Huang, Y. Xu, M. Bai, L. Zhou, S.J. Song, X.B. Wang, Lignans from the seeds of Chinese hawthorn (*Crataegus pinnatifida* var. major NE Br.) against β-amyloid aggregation, Nat. Prod. Res. 32 (2017) 1–8.
[13] L. Zhou, J. Wang, R. Guo, B. Lin, X.B. Wang, X.X. Huang, S.J. Song, Discovery of dihydrobenzofuran neolignans from Rubus ideaus L. with enantioselective anti-$A\beta_{1-42}$ aggregation activity, Bioorg. Chem. 80 (2018) 64–69.
[14] L. Zhou, L.L. Lou, W. Wang, B. Lin, J.N. Chen, X.B. Wang, X.X. Huang, S.J. Song, Enantiomeric 8-*O*-4′ type neolignans from red raspberry as potential inhibitors of β-amyloid aggregation, J. Funct. Foods 37 (2017) 322–329.
[15] Q. Zhang, G. Yan, H. Dai, X. Zhang, C. Li, Z. Zhang, Characterization of Tomentosa cherry (*Prunus tomentosa* Thunb.) genotypes using SSR markers and morphological traits, Sci. Hortic. 118 (2008) 39–47.
[16] C.Y. Zhang, S.H. Shao, Y.L. Shi, Effects on frostbite and inflammation dependablity of Chang Bai *Prunus tomentosa* thumb total flavone, Chin. J. Immunol. 11 (2010) 977–981.
[17] S.K. Kim, H.J. Kim, S.E. Choi, K.H. Park, H.K. Choi, M.W. Lee, Anti-oxidative and inhibitory activities on nitric oxide (NO) and prostaglandin E_2 (COX-2) production of flavonoids from seeds of *Prunus tomentosa* Thunberg, Arch. Pharm. Res. 31 (2008) 424–428.
[18] X.C. Li, D. Ferreira, Y. Ding, Determination of absolute configuration of natural products: theoretical calculation of electronic circular dichroism as a tool, Curr. Org. Chem. 14 (2015) 1678–1697.
[19] B. Jagannadh, S.S. Reddy, R.P. Thangavelu, Conformational preferences of 1,4,7-trithiacyclononane: a molecular mechanics and density functional theory study, J. Mol. Model. 10 (2004) 55–59.
[20] T. Bruhn, A. Schaumlöffel, Y. Hemberger, G. Bringmann, SpecDis: quantifying the comparison of calculated and experimental electronic circular dichroism spectra, Chirality 25 (2013) 243–249.
[21] M.A. Kael, D.K. Weber, F. Separovic, M.A. Sani, Aggregation kinetics in the presence of brain lipids of Aβ(1–40) cleaved from a soluble fusion protein, BBA Biomembranes 9 (2018) 1681–1686.
[22] L. Zhou, J. Wang, R. Guo, B. Lin, X.B. Wang, X.X. Huang, S.J. Song, Discovery of dihydrobenzofuran neolignans from *Rubus ideaus* L. with enantioselective anti-$A\beta_{1-42}$ aggregation activity, Bioorg Chem. 80 (2018) 64–69.
[23] J.B. Klauda, R.M. Venable, J.A. Freites, J.W. O'Connor, D.J. Tobias, C. Mondragonramirez, I. Vorobyov, M.K.A. Jr, R.W. Pastor, Update of the CHARMM all-atom additive force field for lipids: validation on six lipid types, J. Phys. Chem. B 114 (2010) 7830–7843.
[24] F. Manouchehri, Y. Izadmanesh, E. Aghaee, J.B. Ghasemi, Experimental, computational and chemometrics studies of BSA-vitamin B6 interaction by UV–Vis, FT-IR, fluorescence spectroscopy, molecular dynamics simulation and hard-soft modeling methods, Bioorg. Chem. 68 (2016) 124–136.
[25] B. Kumar, S. Sheetal, A.K. Mantha, V. Kumar, ChemInform abstract: recent developments on the structure-activity relationship studies of MAO inhibitors and their role in different neurological disorders, Cheminform 6 (2016) 42660–42683.
[26] L. Zhou, G.D. Yao, X.Y. Song, J. Wang, B. Lin, X.B. Wang, X.X. Huang, S.J. Song, Neuroprotective effects of 1,2-diarylpropane type phenylpropanoid enantiomers from red raspberry against H_2O_2-induced oxidative stress in human neuroblastoma sh-sy5y cells, J. agr. Food Chem. 66 (2017) 331–338.
[27] Y.N. Yang, X.Y. Huang, Z.M. Feng, J.S. Jiang, P.C. Zhang, Hepatoprotective activity of twelve novel 7'-hydroxy lignan glucosides from Arctii Fructus, J. Agr. Food Chem. 62 (2014) 9095–9102.
[28] M. Habib, M. Trajkovic, M.W. Fraaije, The biocatalytic synthesis of syringaresinol from 2,6-dimethoxy-4-allylphenol in one-pot using a tailored oxidase/peroxidase system, Acs. Catal. 8 (2018) 5549–5552.
[29] A.S. Jaufurally, A.R.S. Teixeira, L. Hollande, F. Allais, P.H. Ducrot, Optimization of the laccase-catalyzed synthesis of (±)-syringaresinol and study of its thermal and antiradical activities, Chemistryselect 1 (2016) 5165–5171.
[30] X. Liu, M.H. Yang, X.B. Wang, S.S. Xie, Z.R. Li, D.H. Kim, J.S. Park, L.Y. Kong, Lignans from the root of *Paeonia lactiflora* and their anti-β-amyloid aggregation activities, Fitoterapia 103 (2015) 136–142.
[31] Y.X. Wang, L. Zhou, J. Wang, B. Lin, X.B. Wang, X.X. Huang, S.J. Song, Enantiomeric lignans with anti-β-amyloid aggregation activity from the twigs and leaves of *Pithecellobium clypearia* Benth, Bioorg. Chem. 77 (2018) 579–585.
[32] P.A. Novick, D.H. Lopes, K.M. Branson, A. Esteraschopo, I.A. Graef, G. Bitan, V.S. Pande, Design of β-amyloid aggregation inhibitors from a predicted structural Motif, J. Med. Chem. 55 (2012) 3002–3010.
[33] S. Sharma, B. Nehru, A. Saini, Inhibition of Alzheimer's amyloid-β aggregation in-vitro by carbenoxolone: Insight into mechanism of action, Neurochem. Int. 108 (2017) 481–493.
[34] H.L. Yang, P. Cai, Q.H. Liu, X.L. Yang, F. Li, J. Wang, J.J. Wu, X.B. Wang, L.Y. Kong, Design, synthesis and evaluation of coumarin-pargyline hybrids as novel dual inhibitors of monoamine oxidases and amyloid-β aggregation for the treatment of Alzheimer's disease, Eur. J. Med. Chem. 138 (2017) 715–728.
[35] K. Ikura, K. Takahata, R. Shinagawa, S. Masuda, R. Sasaki, In vitro neurotoxicity of amyloid β-peptide cross-linked by transglutaminase, Cytotechnology 23 (1997) 77–85.